Mustafa Kemal Üniversitesi Tarım Bilimleri Dergisi, 29 (3), 707-723
Mustafa Kemal University Journal of Agricultural Sciences, 29 (3), 707-723
https://dergipark.org.tr/tr/pub/mkutbd
e-ISSN: 2667-7733

ARAŞTIRMA MAKALESİ **RESEARCH ARTICLE**

Comparative analysis of different supervised methods for satellite-based land-use classification: A case study of Reyhanlı

Uydu tabanlı arazi kullanımının sınıflandırılması için farklı denetimli yöntemlerin karşılaştırmalı analizi: Reyhanlı örneği

Mustafa ÖZBULDU[1], Yunus Emre ŞEKERLİ[1]

[1]*Hatay Mustafa Kemal University, Faculty of Agriculture, Department of Biosystems Engineering, Hatay, Türkiye.*

ARTICLE INFO

Article history:
Recieved / Geliş: 16.05.2024
Accepted / Kabul: 12.07.2024

Keywords:
Geographical information systems
Land-use classification
Machine learning
Sentinel-2
Landsat-9

Anahtar Kelimeler:
Coğrafik bilgi sistemleri
Arazi kullanım sınıflandırması
Makine öğrenmesi
Sentinel-2
Landsat-9

Corresponding author/Sorumlu yazar:
Mustafa ÖZBULDU
mustafaozbuldu@mku.edu.tr

ABSTRACT

Satellite-based land-use classification plays a crucial role in various Earth observation applications, ranging from environmental monitoring to disaster management. This study presents a comparative analysis of machine learning techniques applied to land cover classification using Landsat-9 and Sentinel-2 satellite imagery in the Reyhanlı district in southern Türkiye. Three different classification algorithms, Random Forest (RF), Support Vector Machine (SVM), and Maximum Likelihood Classification (MLC), were evaluated for their ability to distinguish different land cover classes. High resolution multispectral satellite imagery processed under the same conditions using Geographic Information System (GIS) software was utilized in this study. Visual inspection and statistical evaluation, including overall accuracy and kappa coefficient, were employed to assess classification performance. The classification of Sentinel-2 and Landsat-9 satellite imagery using different machine learning algorithms resulted in the highest overall accuracy (OA = 0.911, Kappa = 0.879) for Sentinel 2 imagery with the RF algorithm. These findings highlight the importance of satellite image selection and algorithm optimization for accurate land cover mapping. This study provides valuable insights for local planners and authorities and underscores the potential of Sentinel-2 imagery combined with machine learning techniques for effective land-use classification and monitoring.

ÖZET

Uydu tabanlı arazi kullanımının sınıflandırılması, çevre izlemesinden afet yönetimine kadar çeşitli yeryüzü gözlem uygulamalarında hayati bir rol oynamaktadır. Bu çalışma, Türkiye'nin güneyindeki Reyhanlı ilçesinde, Landsat-9 ve Sentinel-2 uydu görüntülerine uygulanan makine öğrenimi tekniklerinin arazi örtüsü sınıflandırması için karşılaştırmalı bir analizini sunmaktadır. Rastgele Orman (RO), Destek Vektör Makinesi (DVM) ve Maksimum Olabilirlik Sınıflandırması (MOS) olmak üzere üç farklı sınıflandırma algoritması, farklı arazi örtüsü sınıflarını ayırt etme başarısı açısından değerlendirilmiştir. Çalışmada, Coğrafi Bilgi Sistemleri (CBS) yazılımı kullanılarak eşit koşullarda işlenmiş yüksek çözünürlüklü multispektral uydu görüntüleri kullanılmıştır. Görsel inceleme ve istatistiksel değerlendirme, genel doğruluk ve kappa katsayısı da dahil olmak üzere sınıflandırma performansını değerlendirmek için kullanılmıştır. Sentinel-2 ve Landsat-9 uydu görüntülerinin farklı makine öğrenmesi algortimaları ile sınıflandırılması sonucunda en yüksek genel doğruluğun (GD = 0.911, Kappa = 0.879) Sentinel-2 görüntüleri için RF algoritması ile elde edildiği tespit edilmiştir. Bulgular, uydu görüntüsü seçiminin ve algoritma optimizasyonunun doğru arazi örtüsü haritalaması için önemini vurgulamaktadır. Bu çalışma, yerel planlamacılar ve otoriteler için önemli bir bakış açısı sunmakta ve Sentinel-2 görüntüleri ile makine öğrenme tekniklerinin etkili arazi kullanımı, sınıflandırması ve izlenmesi için potansiyelini ortaya koymaktadır.

Cite/Atıf Özbuldu, M., & Şekerli, Y.E. (2024). Comparative analysis of different supervised methods for satellite-based land-use classification: A case study of Reyhanlı. *Mustafa Kemal Üniversitesi Tarım Bilimleri Dergisi, 29* (3), 707-723. https://doi.org/10.37908/mkutbd.1485236

INTRODUCTION

For seventy years, obtaining information about land-use without physical contact, through satellite imagery, has been a critical component in various Earth observation applications (Fröhlich et al., 2013). These applications including environmental monitoring, land-use change, urban planning, crop yield estimation, disaster management, carbon modeling, and forest management (Zhu et al., 2012; Fröhlich et al., 2013; Paul & Kumar, 2019; Leeuwen and Kovacs, 2020).

The demand for land-use maps has increased due to their role in land and resource planning and management, with land-use maps delineating biophysical land-use maps depicting human activities within specific land-use types. Different methods have been developed to map land-use patterns and changes using satellite data, including both traditional ground-based mapping and satellite-based approaches (Talukdar et al., 2020; Darem et al., 2023; Irvem & Ozbuldu, 2023). Due to the time-consuming, costly, and personnel-intensive nature of manual digitization of land-use or land surveying methods, new automated digitalization methods that extract land-use information using remote sensing and satellite imagery data are increasingly gaining importance (Fröhlich et al., 2013; Geçen, 2019). Remote sensing data are pivotal tools for monitoring Earth's surface features and understanding the spatio-temporal variability of land surfaces. With the progression of remote sensing techniques and the integration of microwave sensors, satellites furnish data across diverse spatial and temporal scales. This technology offers a cost-effective means of rapidly acquiring land-use information, significantly reducing the expenses compared with traditional ground surveys (Paul & Kumar, 2019; Bouslihim et al., 2022; Dhakal et al., 2022; Zhang & Li, 2022). Given the capability to acquire swift, regular, and precise data through remote sensing systems, satellite imagery stands out as a significant source for generating land-use maps utilizing image classification techniques (Topaloglu et al., 2016).

The global availability of imagery from cost-free platforms such as Landsat-9 and Sentinel-2 underscores their status as the most extensively used optical remote sensing satellites, driving the need for increasingly efficient and accurate classification techniques to extract meaningful insights from the advancing technology (Paul & Kumar, 2019; Bouslihim et al., 2022). However, accurate classification of land-use from satellite imagery poses several challenges due to the complexity and variability of terrestrial surfaces, as well as the influence of atmospheric conditions and sensor characteristics on remote sensing data (Talukdar et al., 2020; Abdelmajed & Juszczak, 2024). Traditional classification methods (band ratios, pixel comparing with reference spectra etc.) have limitations in capturing the intricate spectral, spatial, and temporal patterns present in satellite imagery (Talukdar et al., 2020; Turner et al., 2022). In contrast, machine learning techniques, with their ability to learn from data and adapt to diverse patterns, have demonstrated significant promise in overcoming these challenges and achieving higher classification accuracies (Razafinimaro et al., 2022).

Numerous classifiers, including maximum likelihood, neural networks, decision trees, support vector machines, and random forest, have been developed and evaluated for land-use classification (Zhu et al., 2012). In the field of machine learning, methodologies are commonly categorized into two primary sub-types: supervised and unsupervised techniques (Talukdar et al., 2020). Nonparametric methods such as Support Vector Machines (SVM) and Random Forests (RF), along with parametric approaches like the Maximum Likelihood Classifier (MLC), have proven effective in remote sensing image classification (Deilmai et al., 2014; Zhang et al., 2018; Gunlu, 2021; Saboori et al., 2022). In addition, SVM and RF are becoming popular in image classification research due to their robust capacity to effectively manage the challenges posed by unbalanced data distributions (Leeuwen & Kovacs, 2020).

In the realm of remote sensing, the SVM emerges as a foremost non-parametric classifier, offering unparalleled potential for accurate land-use classification, owing to its capability to operate without presumptions about the underlying data distribution (Paul & Kumar 2019; Leeuwen & Kovacs, 2020;). RF stands out as the prevailing classification approach documented in the literature, leveraging class-specific statistics within each band as a

normally distributed function whereas MLC classification is based on a parametric approach that assumes the selected classes of signature in the normal distribution (Deilmai et al., 2014; Dang et al., 2020; Leeuwen & Kovacs, 2020; Gunlu, 2021). According to the comparison performed by Mondal et al. (2012) between SVM and MLC for land-use classification, non-parametric SVM outperformed MLC. Gosh and Joshi (2014) found that highly accurate and similar classification results are offered by SVM and RF algorithms. Compared with other machine learning approaches, SVM and RF are generally regarded as the optimal methods for land-use mapping (Deilmai et al., 2014; Camargo et al., 2019; Jamali, 2019).

This study provides a comprehensive evaluation of the accuracy of different machine learning techniques for land-use classification from satellite imagery. We focus on assessing the performance of various supervised classifiers, including SVM, RF, MLC, in accurately discriminating between different land-use classes. These classifiers represent a diverse range of machine learning paradigms, each with unique strengths and characteristics suitable for handling different types of land-use classification tasks. The evaluation was conducted on a diverse set of satellite imagery datasets covering various geographical regions and land-use types, including Bare Land, Urban, Cropland (Planted), Cropland (Unplanted), and Water Bodies. Each dataset presents its own set of challenges and opportunities, allowing for a comprehensive assessment of classifier performance under different environmental conditions and land-use compositions.

MATERIALS and METHODS

Description of the study area

The study area is a district located in the southern part of Türkiye (Figure 1). The district covers an area of 367 km² and has an average elevation of 160 m above sea level. 80% of the district's surface area is composed of flatlands. The Afrin River runs through the northern part of the district and joins the Orontes River in the Amik Plain to the west. The Mediterranean climate prevails in the study area. The average annual temperature was 18°C, and the average annual precipitation was 600 mm (Bilginer, 2023). Alluvial and Red Mediterranean soils are common in Reyhanlı. Alluvial soils, which constitute 65% of the district's total land area, are highly suitable for agricultural production. Approximately 60% of the agricultural land in the district is used for irrigated agriculture (Atasoy & Geçen, 2014).

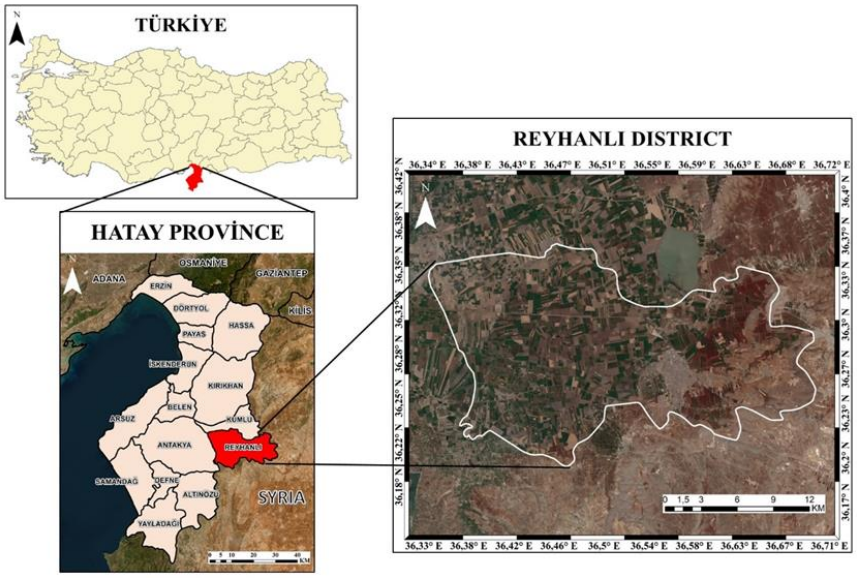

Figure 1. The location of the study area (Reyhanlı District)

Şekil 1. Çalışma alanının konumu (Reyhanlı İlçesi)

Satellite data

Remote sensing techniques are becoming increasingly valuable for mapping land-use over large and remote areas. Researchers can gain valuable insight into land-use patterns using spectral bands from different wavelengths of the electromagnetic spectrum. However, high-resolution imagery of the Earth's surface is essential for accurate land-use classification, and such data are not always readily available. This study aims to compare the performance and assess the feasibility of using high-resolution multispectral imagery for land-use classification. To achieve this objective, two freely available satellite products with 5% cloud cover were used (Table 1). Satellite imagery was acquired in the summer season to include as many different land use classes as possible in the plain, taking into account the low cloud cover. In July, when the images were obtained, there are generally second crop maize, cotton and soybean on the fields that can be classified as green in imagery.

Landsat-9 is a satellite, which has been instrumental in Earth observation and remote sensing. It is equipped with two advanced instruments: the Thermal Infrared Sensor-2 (TIRS-2) and the Operational Land Imager-2 (OLI-2) (McCorkel et al., 2018). These instruments play a vital role in capturing multispectral images that are essential for various applications such as land-use analysis, remote sensing, and environmental monitoring. The data collected by Landsat-9 are instrumental in modeling land surface processes and monitoring changes in the Earth's surface over time (Cristóbal et al., 2018).

Table 1. Landsat-9 and Sentinel-2's main characteristics

Çizelge 1. Landsat-9 ve Sentinel-2'nin temel özellikleri

Satellite	Bands	Spectral range (µm)	Pixel size (m)	Revisit time (days)	Granule ID
Landsat-9	Band 1-Coastal/Aerosol	0.433–0.453	30	16	LC09_L2SP_174035_20230724_20230802_02_T1
	Band 2-Blue	0.450–0.515	30		
	Band 3-Green	0.525–0.600	30		
	Band 4-Red	0.630–0.680	30		
	Band 5-NIR	0.845–0.885	30		
	Band 6-SWIR 1	1.560–1.660	30		
	Band 7-SWIR 2	2.100–2.300	30		
	Band 8-Panchromatic	0.500–0.680	15		
	Band 9-Cirrus	1.360–1.390	30		
	Band 10-TIRS 1	10.30–11.30	100		
	Band 11-TIRS 2	11.50–12.50	100		
Sentinel-2	Band 1-Coastal	0.433–0.453	60	5	S2B_MSIL1C_20230724T081609_N0509_R121_T37SBA_20230724T094100
	Band 2-Blue	0.457–0.522	10		
	Band 3-Green	0.542–0.577	10		
	Band 4-Red	0.650–0.680	10		
	Band 5-Veg. Red Edge	0.679–0.718	20		
	Band 6-Veg. Red Edge	0.732–0.747	20		
	Band 7-Veg. Red Edge	0.773–0.793	20		
	Band 8-NIR	0.784–0.899	10		
	Band 8A-Veg. Red Edge	0.855–0.885	20		
	Band 9-Water Vapor	0.935–0.955	60		
	Band 10-Cirrus	1.360–1.390	60		
	Band 11–SWIR 1	1.565–1.655	20		
	Band 12–SWIR 2	2.100–2.280	20		

Sentinel-2 is a high-resolution (10 m) satellite imaging system that captures imagery in 13 bands across the visible, near-infrared, and shortwave infrared parts of the spectrum (Tricht et al., 2018). The Sentinel-2 satellite offers several advantages that make it a valuable tool for various applications. One key advantage is its decametric

resolution in terms of space and time, which provides a ground sample distance of up to 10 m and a revisit time of five days (Khaliq et al., 2019). This high temporal availability of Sentinel-2 images allows for frequent monitoring, aiding in the development of systems to keep maps up-to-date (Helber et al., 2019). Sentinel-2's high temporal frequency and spatial resolution have significantly contributed to phenological research and improved land mapping research (Mishra et al., 2020).

Google Earth Engine (GEE) is a cloud-based platform that facilitates rapid processing of geospatial data. It provides access to a vast array of geospatial datasets, including satellite imagery, radar data, land-use maps, and more. Additionally, GEE offers powerful processing tools that enable users to analyze and visualize these datasets efficiently (Wang et al., 2019). The Google Earth Engine provides access to a large number of processed satellite images, including Landsat-9 and Sentinel-2 (Tariq et al., 2021; Gašparović et al., 2021; Castillo et al., 2022). Landsat-9 Collection 2 Tier 1 top-of-atmosphere (TOA) reflectance and Sentinel-2 level (L2A) bottom-of-atmosphere (BOA) calibrated satellite images of the study area were obtained using the GEE cloud platform. While obtaining Landsat-9 and Sentinel-2 images, care was taken to ensure that the cloudiness was less than 5% and that they were obtained on recent dates. RGB and Colour Infrared (NIR, R, G) composite images were also created using the GEE cloud program (Figure 2). The obtained images were transferred to ArcGIS 10.8 GIS software for the application of classification algorithms. To observe the effect of different spatial resolutions of the images, no pan sharpening method was applied to Landsat-9 images.

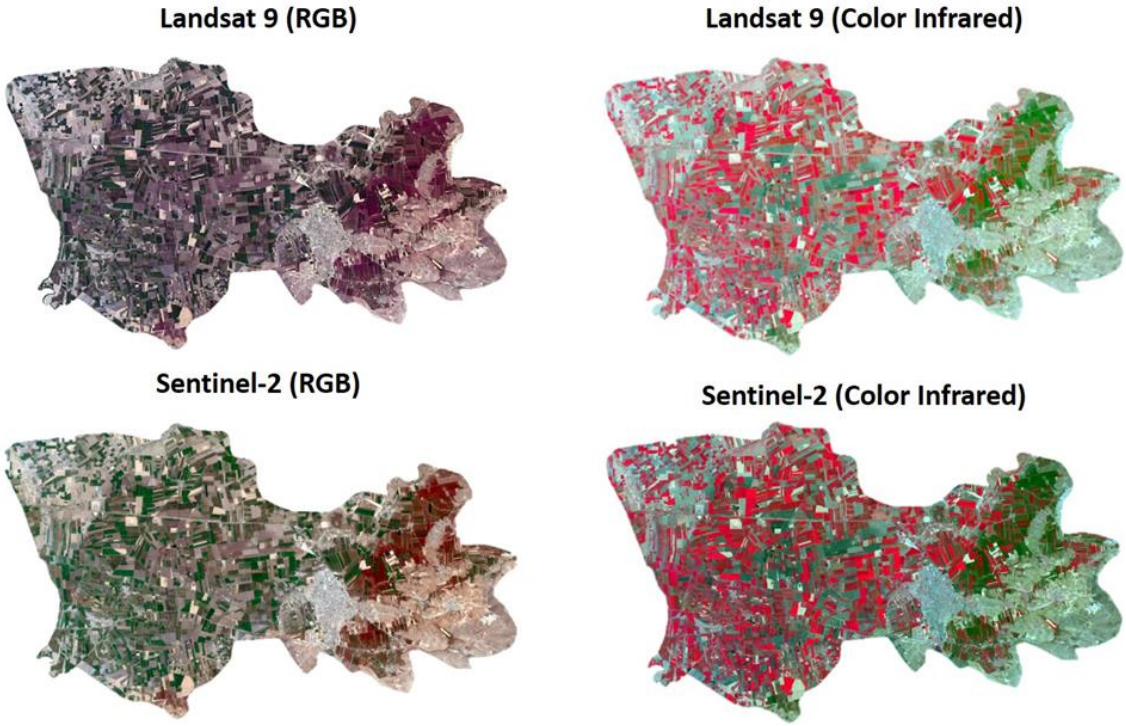

Figure 2. Landsat-9 and Sentinel-2 satellite images for Reyhanli District

Şekil 2. Reyhanlı İlçesi için Landsat-9 ve Sentinel-2 uydu görüntüleri

Methodology for land-use classification

In this study, a framework was developed to compare the performance and applicability of different classification methods available in ArcGIS software using images from two different satellites (Figure 3). The classification procedure was carried out with three different supervised methods (RF, SVM and MLC), and land-use prediction performances were compared. GPS-verified sample points in the study area for five different land-use classes (Bare Land, Cropland (Planted), Cropland (Unplanted), Water Body, Urban) were used to train and test the models (Table

2). Of these sample points, 70% were used for training the models and 30% were used for testing the models. The success of the classified maps obtained for both satellite images was evaluated by calculating the overall accuracy and kappa accuracy.

Table 2. Number of test and training samples for each class

Çizelge 2. Her sınıf için test ve eğitim örneklerinin sayısı

Class	Training Data	Testing Data
Bare Land	70	30
Cropland (Planted)	150	70
Cropland (Unplanted)	130	51
Water Body	20	10
Urban	50	19
Total	420	180

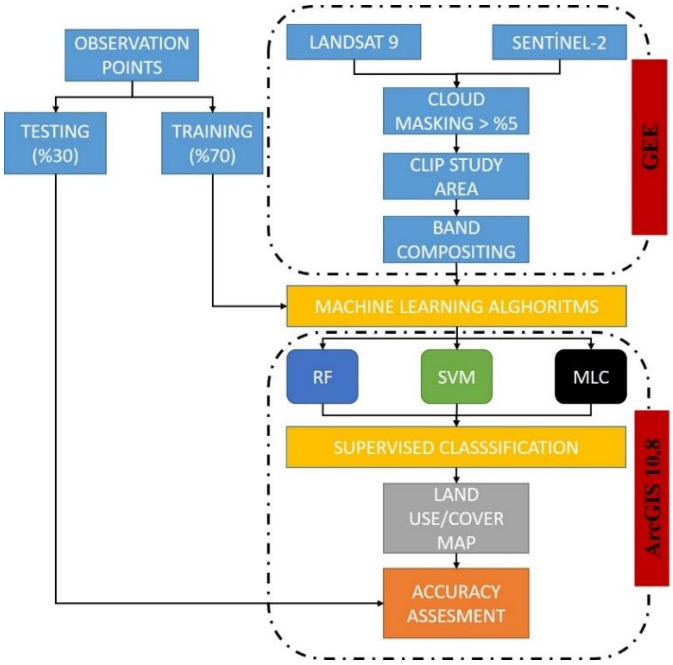

Figure 3. Flow chart of the study

Şekil 3. Çalışmanın akış şeması

Classification methods

Random Forest (RF)

Random forest/random tree is a robust machine learning algorithm widely used across various fields due to its accuracy and robustness. It is an ensemble learning method that builds multiple decision trees during training and outputs the mode of the classes for classification or the average prediction for regression tasks (Breiman, 2001). One of the key strengths of the RF algorithm is its effectiveness in handling large datasets with high dimensionality and numerous input attributes (Cerrada et al., 2016). The algorithm is also known for its ability to resist overfitting, making it suitable for processing data with missing values, noise, and outliers (Ma & Fan, 2017). The RF algorithm has gained significant attention in the fields of Geographic Information Systems (GIS) and Remote Sensing (RS) due to its effectiveness in handling complex datasets and improving classification accuracy (Peng et al., 2021). The application of RF in GIS and RS extends to various domains, including agriculture, forest monitoring, and land-use classification (Li & Xu, 2021; Wei et al., 2023)

Support Vector Machine (SVM)

Support Vector Machine is a widely used classification methodology in data mining and machine learning. SVMs achieve this by identifying an optimal hyperplane within a high-dimensional space. This hyperplane effectively separates data points belonging to distinct classes, allowing for accurate categorization of new data instances (Daribayev et al., 2021). To establish the hyperplane, SVMs strategically select a subset of data points termed support vectors. The margin, which represents the distance between the support vectors and the hyperplane, is maximized by the SVM algorithm. This optimization process ensures robust classification performance (Vapnik, 2013). SVM's ability to handle large datasets efficiently is a key factor contributing to its popularity. In the field of GIS, SVM has been widely used for tasks such as image classification, object recognition, and land-use mapping (Morgan et al., 2022).

Maximum Likelihood Classifier (MLC)

Maximum Likelihood Classification is a widely used method in GIS and RS for image classification. MLC is a supervised classification technique that aims to assign each pixel in an image to the class that maximizes the likelihood of the pixel's spectral signature belonging to that class. This method is particularly effective in identifying different land-use types such as urban areas, vegetation, water bodies, and hills (Sisodia et al., 2014). In the field of remote sensing, MLC has been extensively applied for various purposes such as mapping vegetation, monitoring land-use changes, and classifying different types of terrain (Rakwatin et al., 2010). A qualitative assessment of the spectral reflectance variance and covariance for each class is performed by MLC, as described in Equation 1.

$$L = \frac{1}{(2\lambda)^{\frac{n}{2}}|\Sigma_k|^{\frac{1}{2}}} exp\left|\frac{1}{2}(x-\mu_k)\sum_k^{-1}(X-\mu_k)^t\right| \quad \textbf{(1)}$$

where; n represents spectral resolution, L represents the likelihood of X belonging to class k, X represents belonging to class k, μ_k represents the mean vector of class k, and Σ_k represents the variance-covariance matrix of class k.

Classification accuracy

Accuracy assessment is one of the most important steps in land-use classification. This assessment ensures that the sampled pixels are effectively assigned to the relevant land-use classes. The accuracy assessment of the land-use classification is done by calculating a confusion matrix by comparing the calculated land-use information with the test data. A confusion matrix serves as a valuable tool for measuring the overall accuracy and Kappa coefficient (Ahady & Kaplan, 2022). Overall accuracy refers to the ratio of correctly classified reference samples to the total number of reference samples (Eq.2)

$$Overall\ Accuracy = \frac{no\ of\ correct\ classified\ feature}{total\ feature} \times 100 \quad \textbf{(2)}$$

Kappa accuracy, also known as the Kappa coefficient, is a statistical measure that assesses the agreement between observed and predicted classifications while considering the agreement occurring by chance (Eq.3). It is widely used in various fields such as remote sensing, land-use classification, and image processing to evaluate the accuracy of classification results (Ahmad et al., 2021). The Kappa coefficient provides a more robust assessment of accuracy than overall accuracy by incorporating both diagonal and off-diagonal elements, making it a valuable metric in classification tasks (Islami et al., 2022).

$$\text{Kappa Accuracy } (\kappa) = \frac{N\sum_{i=1}^{r} x_{ii} - \sum_{i=1}^{r}(x_{i+} \times x_{+i})}{N^2 - \sum_{i=1}^{r}(x_{i+} \times x_{+i})} \quad \textbf{(3)}$$

where; r denotes the total number of rows in the error matrix, x_{ii} signifies the count of observations at the intersection of row i and column i, x_{i+} represents the sum of observations within row i, x_{+i} represents the total of observations in column i, and N represents the total number of observations included in the matrix.

RESULTS and DISCUSSIONS

Land-use classification results

Landsat-9 and Sentinel-2 satellite images were classified using RF, SVM, and MLC algorithms, and the obtained classification maps are shown in Figure 4. A total of six classification maps were created and five different land-use classes were evaluated. On the basis of general visual inspection, it was found that the classification performance of combinations using Sentinel-2 imagery was better than classification using Landsat-9 imagery. In general, when compared with other classification combinations, Sentinel 2+RF was found to be more successful. It was observed that the Sentinel-2+SVM misclassified some Cropland (Unplanted) areas as Bare Land, and some Cropland (Planted) areas as Water Body. The Sentinel-2+MLC was found to often confuse Bare Land, Urban, and Cropland (Unplanted) areas when classifying them. When the classifications performed with Landsat-9 imagery were evaluated, it was observed that the most successful classification result was achieved with the Landsat-9+RF combination. In particular, the Landsat-9+MLC tended to misclassify Cropland (Planted) areas as Water Body. The reason why Sentinel-2 imagery were more successful than Landsat-9 images are the presence of red edge bands and their higher spatial resolution. It was considered that visual control at a higher spatial scale would allow for better analysis and comparison of the classification results, so images from four different locations (Figure 4-8) were evaluated separately on the study area.

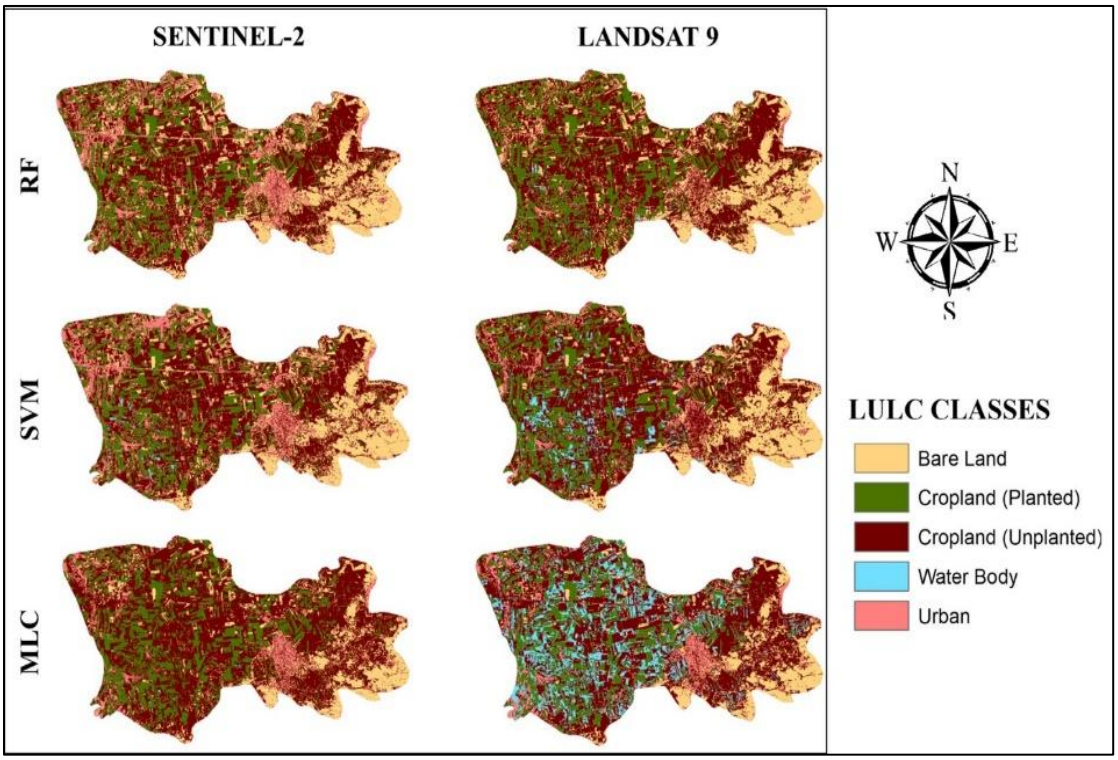

Figure 4. Land-use classification maps obtained by processing Sentinel-2 and Landsat-9 satellite imagery with RF, SVM and MLC

Şekil 4. Sentinel-2 ve Landsat-9 uydu görüntülerinin RF, SVM ve MLC ile işlenmesiyle elde edilen arazi kullanım sınıflandırma haritaları

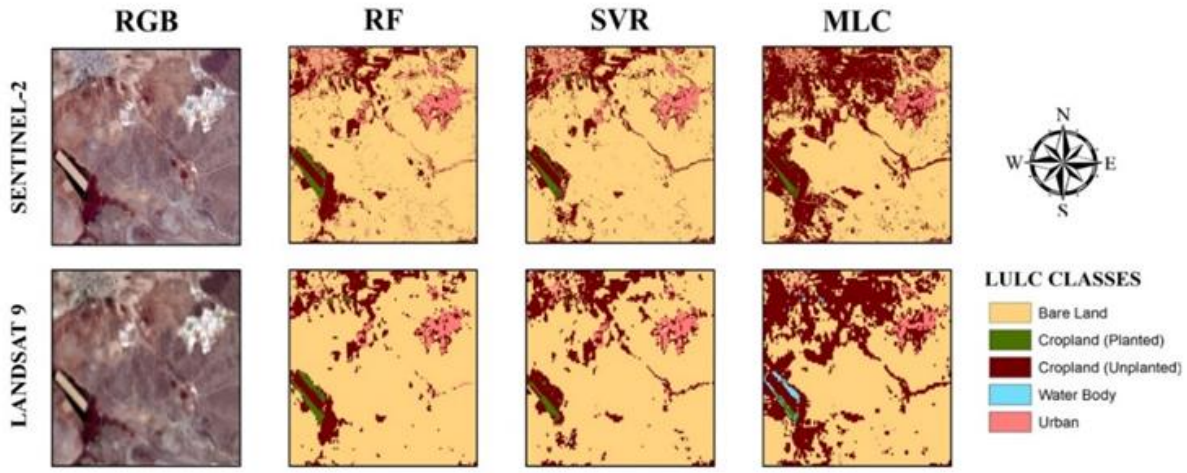

Figure 5. Comparison of classification maps for Bare Land class weighted location

Şekil 5. Çıplak Arazi sınıfı açısından yoğun konum için sınıflandırma haritalarının karşılaştırılması

The eastern part of the Reyhanlı district is depicted in Figure 5 and is mainly characterized by the Bare Land class. As can be observed from the figures, Sentinel-2+RF and Sentinel-2+SVM successfully distinguished both Bare Land and other classes. However, the RF and SVM models for Landsat-9 were successful in the classification of Bare Land, while they were not as successful in the classification of other classes, particularly Urban. In addition, the MLC models for both satellite imageries were not sufficiently successful in differentiating between Bare Land and Cropland (Unplanted). It was also found that the Landsat-9+MLC misclassified Cropland (Planted) areas as Water Body.

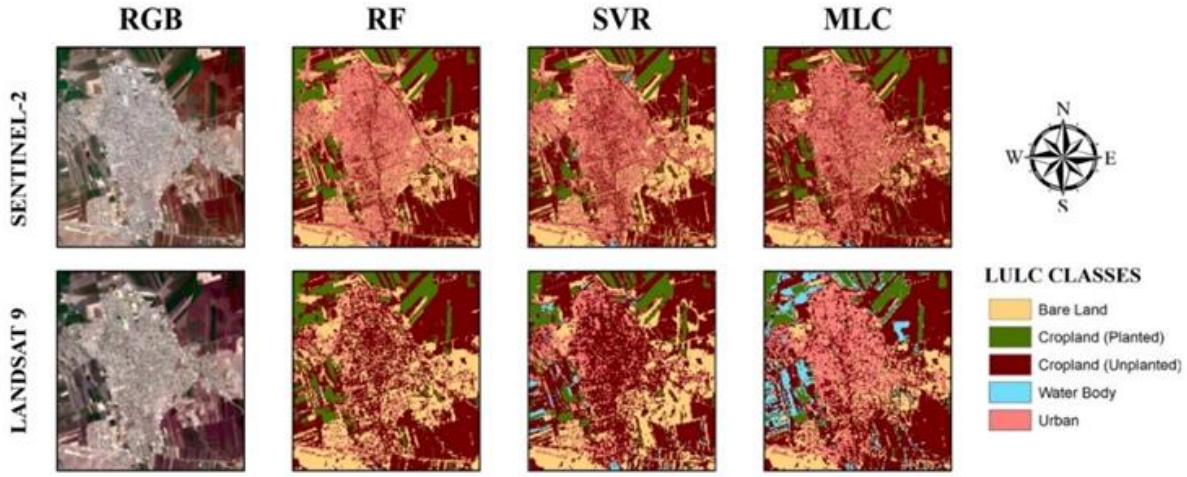

Figure 6. Comparison of classification maps for Urban class weighted location

Şekil 6. Kent sınıfı açısından yoğun konum için sınıflandırma haritalarının karşılaştırılması

As depicted in Figure 6, a location in the city center of the Reyhanlı district, where the urban class is more abundant. The RF, SVM, and MLC models were found to be successful in predicting urban areas for the Sentinel-2 imagery. Remarkably, the Sentinel-2+RF was also found to be very accurate in predicting all other land-use classes. The Landsat-9+RF was determined to have difficulty distinguishing between Urban and Bare Land, while the Landsat-9+SVM struggled to differentiate between Urban and Cropland (Unplanted) classes. In contrast, Urban areas were successfully classified by the Landsat-9+MLC, whereas Cropland (Planted) areas were misclassified as Water Bodies.

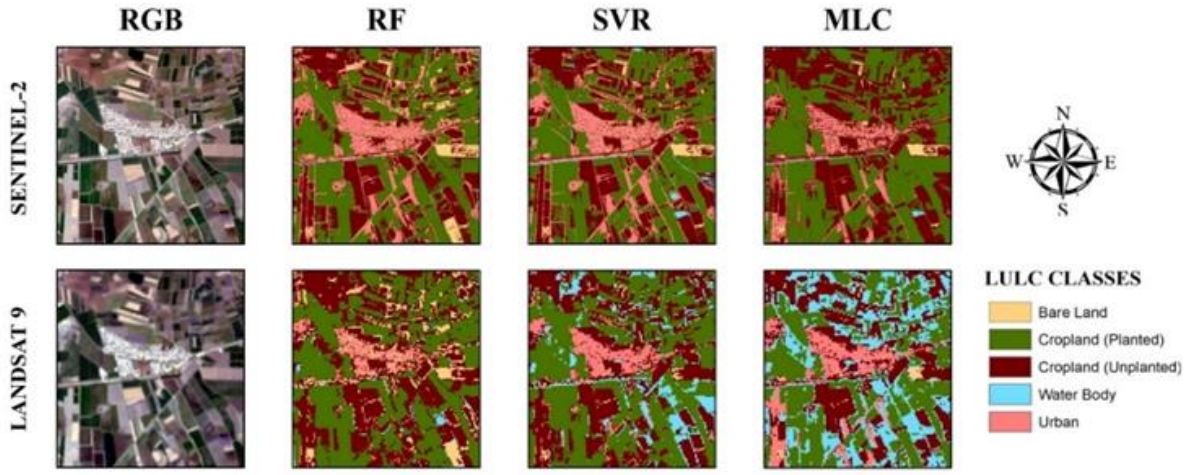

Figure 7. Comparison of classification maps for Cropland (Planted) class weighted location
Şekil 7. Tarım alanı (Ekili) sınıfı açısından yoğun konum için sınıflandırma haritalarının karşılaştırılması

As shown in Figure 7, a region characterized by the prevalence of the Cropland (Planted) class in the southeast of Reyhanlı district. It is noteworthy that the Sentinel-2+RF and Sentinel-2+SVM performed better in classifying these areas. In contrast, the Landsat-9+RF struggled to differentiate between Urban and Bare Land. Furthermore, Landsat-9+SVM and Landsat-9+MLC exhibited difficulties in separating Cropland (Planted) from Water Body leading to unsuccessful classifications.

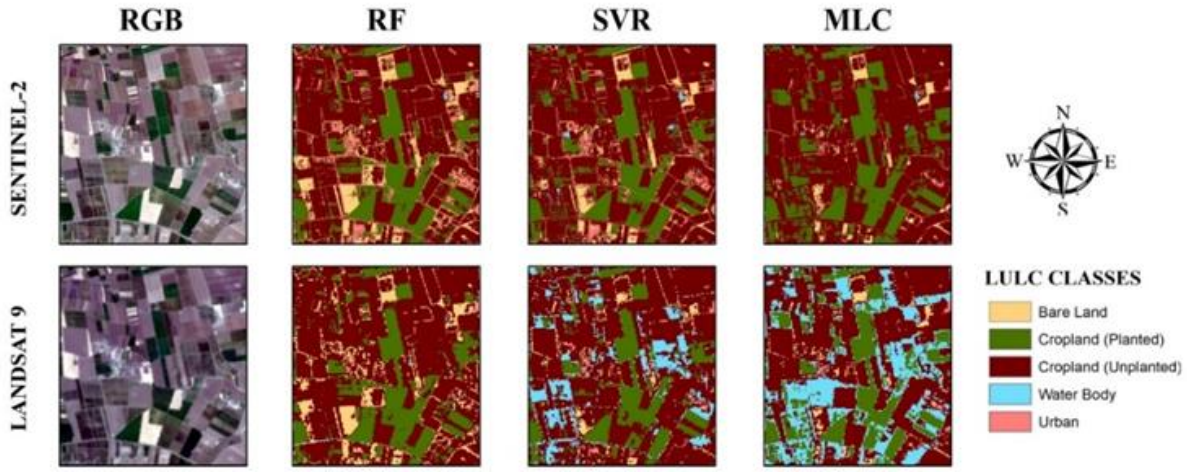

Figure 8. Comparison of classification maps for Cropland (Unplanted) class weighted location
Şekil 8. *Tarım alanı (Ekilmemiş) sınıfı açısından yoğun konum için sınıflandırma haritalarının karşılaştırılması*

The central part of the Reyhanlı district, where the Cropland (Unplanted) class is more prevalent, is shown in Figure 8. Sentinel-2+RF, Sentinel-2+SVM, Sentinel-2+MLC, and Landsat-9+RF were generally successful in classifying Cropland (Planted) areas. However, they had difficulty in distinguishing some areas of Cropland (Unplanted) from Bare Land. Additionally, it was observed that Sentinel-2+SVM and Sentinel-2+MLC classified some Cropland (Planted) areas as Water Body. Landsat-9 and Sentinel-2+MLC were found to be insufficiently successful in classification.

Accuracy assessment of the classification

The performance of each land-use class was evaluated based on the confusion matrix results for overall accuracy and Kappa coefficient (Table 3). Comparison of the RF model classification results of Landsat-9 and Sentinel-2 imagery revealed that the Sentinel-2+RF (OA = 0.911, Kappa = 0.879) outperformed Landsat-9+RF (OA = 0.878, Kappa = 0.832). The Sentinel-2+RF slightly outperformed Landsat-9+RF (67/70) in the classification of Cropland (Planted) (68/70). Both combinations classified Bare Land with the same accuracy level. The Sentinel-2+RF achieved highly successful predictions for the Water Body (10/10) and Urban (19/19) classes. On the other hand, the Landsat-9+RF (41/51) gave more successful predictions for the Cropland (Unplanted) class than the Sentinel-2+RF (38/51).

In comparing the SVM model classification results for Landsat-9 and Sentinel-2 imagery, it was observed that the Sentinel-2+SVM (OA = 0.900, Kappa = 0.864) outperformed the Landsat-9+SVM (OA = 0.862, Kappa = 0.810). The Sentinel-2+SVM was slightly superior to the Landsat-9+SVM (67/70 vs. 66/70) for the classification of Cropland (Planted). Both combinations classified the Bare Land and Cropland (Unplanted) classes with the same accuracy level. The Sentinel-2+SVM achieved better prediction accuracy for the Water Body (10/10) and Urban (16/19) classes. In the case of the use of MLC model, the classification results showed a clear advantage for the Sentinel-2 imagery. The Sentinel-2+MLC achieved a higher overall accuracy (OA = 0.900, Kappa = 0.862) compared to the Landsat-9+MLC (OA = 0.861, Kappa = 0.809). In this regard, the Sentinel-2+MLC performed exceptionally well in classifying the Water Body (10/10) and Urban (15/19) classes. Whereas the Landsat-9+MLC provided better accuracy in classifying Bare Land (28/30). In contrast, both models achieved similar classification accuracies for the Cropland (Unplanted) class.

A comprehensive evaluation of the results revealed that Sentinel-2 imagery outperformed Landsat 9 imagery across all three supervised classification models. The key factor contributing to this advantage lies in the difference in spatial resolution. High-resolution pixels in Sentinel-2 imagery enable more accurate identification of land-use types. Conversely, lower-resolution pixels in Landsat-9 data tend to generalize heterogeneity within a single pixel, hindering precise classification (Zhao et al., 2014). The overall evaluation revealed that the models struggled to distinguish between Cropland (unplanted) and Bare Land classes. This is probably due to the similar reflectivity of these land-use types (Bouslihim et al., 2022). Furthermore, the misclassification of Cropland (Planted) areas as Water Body is likely due to the image acquisition date in July, coinciding with a potential irrigation period for planted crops. This highlights the importance of considering image acquisition timing in relation to land-use characteristics for improved classification accuracy. As Landsat-9 imagery has only recently become available, there are relatively few land-use classification studies using these images. Therefore, the results of studies that have used Landsat-8 data are also considered for discussion in this study. Several studies have reported the potential advantages of Sentinel-2 imagery compared to Landsat for land-use applications. Htitiou et al. (2019) used Landsat-8 and Sentinel-2 imagery to classify irrigated agricultural areas in Morocco. They revealed that Sentinel-2 (OA=0.93 and Kappa=0.91) outperformed Landsat-8 (OA=0.90 and Kappa=0.88) in terms of classification accuracy. Similarly, Nyamekye et al. (2021) compared the classification performance of Landsat-8 and Sentinel-2 imagery for mapping small-scale mining in Ghana. The results indicated that Sentinel-2 (OA = 0.95 and Kappa = 0.94) outperformed Landsat-8. Bouslihim et al. (2022) used RF and SVM models to classify land-use using Sentinel-2 and Landsat-9 imagery. Also Sentinel-2 combinations were more accurate at prediction than Landsat-9 combinations. Manessa et al. (2024) investigated changes in reef habitats on Derawan Island, Indonesia, using Landsat-9 and Sentinel-2 imagery with different classification models. According to the results, Sentinel-2 imagery were found to be more successful than Landsat-9 imagery due to the significant effect of spatial resolution and image quality on classification accuracy. In accordance with the results of current study, previous studies also recommended the use of Sentinel-2 imagery for land-use mapping due to the higher resolution and accuracy when combined with different classification models.

Table 3. Confusion matrix for combinations of supervised methods with Sentinel-2 and Landsat-9 imagery with predictions (columns) and reference samples (rows)

Çizelge 3. Sentinel-2 ve Landsat-9 görüntüleri ile denetimli yöntemlerin kombinasyonları için karışıklık matrisi, tahminler (sütunlar) ve referans örnekler (satırlar)

Model	ClassValue	Bare Land	Cropland (Planted)	Cropland (Unplanted)	Water Body	Urban	*OA*	*Kappa*
Sentinel-2+RF	Bare Land	**29**	0	11	0	0	**0.911**	0.879
	Cropland (Planted)	0	**68**	0	0	0		
	Cropland (Unplanted)	1	2	**38**	0	0		
	Water Body	0	0	0	**10**	0		
	Urban	0	0	2	0	**19**		
Landsat-9+RF	Bare Land	**29**	0	8	1	2	0.878	0.832
	Cropland (Planted)	0	**67**	1	1	0		
	Cropland (Unplanted)	1	3	**41**	2	2		
	Water Body	0	0	0	**6**	0		
	Urban	0	0	1	0	**15**		
Sentinel-2+SVM	Bare Land	**29**	0	11	0	0	**0.900**	0.864
	Cropland (Planted)	0	**67**	0	0	0		
	Cropland (Unplanted)	1	3	**38**	0	1		
	Water Body	0	0	0	**10**	0		
	Urban	0	0	2	0	**18**		
Landsat-9+SVM	Bare Land	**29**	0	9	1	2	0.862	0.810
	Cropland (Planted)	0	**66**	1	1	0		
	Cropland (Unplanted)	1	4	**38**	2	1		
	Water Body	0	0	2	**6**	0		
	Urban	0	0	1	0	**16**		
Sentinel-2+MLC	Bare Land	**25**	0	8	0	0	**0.900**	0.862
	Cropland (Planted)	0	**69**	0	0	0		
	Cropland (Unplanted)	5	1	**43**	0	4		
	Water Body	0	0	0	**10**	0		
	Urban	0	0	0	0	**15**		
Landsat-9+MLC	Bare Land	**28**	0	7	1	1	0.861	0.809
	Cropland (Planted)	0	**66**	0	1	0		
	Cropland (Unplanted)	2	0	**42**	1	6		
	Water Body	0	4	2	**7**	0		
	Urban	0	0	0	0	**12**		

* OA: Overall Accuracy, RF: Random Forest, SVM: Support Vector Machine, MLC: Maximum Likelihood Classifier

RF was found to be superior to SVM and MLC in both visual and statistical comparisons. In particular, the SVM and MLC classifications showed significant confusion between Cropland (planted) and Water Body classes, as well as Cropland (unplanted) and Bare Land classes. This highlights the advantage of RF in dealing with complex classification tasks. This may be due to its ability to handle large datasets efficiently and reduce overfitting, contributing to superior performance (Shi et al., 2019). Numerous previous studies on this topic have reported that the RF model is more successful than other models. Toosi et al. (2019) found that the RF model achieved superior performance for mangrove cover identification in Iran using various machine learning techniques. Adam et al. (2021) obtained an overall accuracy of 93.07% for RF while SVM provided 91.80% for land-use classification in East Africa. Similarly, Adugna et al. (2022) reported an accuracy advantage of 3% for RF compared to SVM in large-scale

land-use mapping across Africa. In another study conducted in South Africa, Jombo and Adelabu (2023) investigated the effectiveness of RF and k-Nearest Neighbor (kNN) models for land-use classification using Landsat 9, Landsat 8, and Sentinel-2 imagery. The study found that RF combinations achieved OA values of 0.92-0.96, outperforming the kNN model. Palanisamy et al. (2023) evaluated Landsat-9 and Sentinel-2 imagery using different classification methods in Delhi, India. As a result of the evaluation of all input combinations for both Landsat-9 and Sentinel-2 datasets, they found that the RF model (OA = 0.96) outperformed the other models. Similar to the results of the current study, these studies show that preferring the RF model for land-use classification provides more accurate predictions.

In this study, machine learning algorithms including RF, SVM and MLC were used to assess the capability of Landsat-9 and Sentinel-2 imagery for land-use mapping. The focus area was the Reyhanlı district in southern Türkiye. The same training and validation data were used under identical processing conditions to produce six land-use maps, three from each satellite source. These maps were then compared both visually and statistically. The evaluation revealed that the combination of RF and Sentinel-2 imagery produced the most accurate land-use map (OA = 0.91, Kappa = 0.88). This combination had significantly fewer misclassifications compared to other algorithms and satellite image pairings. Conversely, the MLC algorithm applied to Landsat-9 imagery produced the least accurate map (OA = 0.861, Kappa = 0.809). The findings of this study provide valuable insights into the utilization of satellite imagery for land-use mapping and monitoring. The results suggest that Sentinel-2 imagery combined with the RF algorithm could be more effective for classification. Future research should extend these findings by incorporating a wider range of satellite imagery and classification algorithms, including deep learning methods. In addition, evaluating imagery with different spatial and temporal resolutions and using more ground truth data to assess accuracy would strengthen future studies. Further development of these aspects will allow researchers to optimize the selection of satellite imagery and algorithms for improved land-use classification, particularly in the identification of cultivated agricultural areas. Eventually, such advances will contribute to the continued development and optimization of satellite imagery in land-use mapping and monitoring applications.

STATEMENT OF CONFLICT OF INTEREST

The authors declare no conflict of interest for this study.

AUTHOR'S CONTRIBUTIONS

The contribution of the authors is equal.

STATEMENT OF ETHICS CONSENT

Ethical approval is not applicable, because this article does not contain any studies with human or animal subjects.

REFERENCES

Abdelmajeed, A.Y.A., & Juszczak, R. (2024). Challenges and limitations of remote sensing applications in Northern Peatlands: present and future prospects. *Remote Sensing*, *16* (3), 591. https://doi.org/10.3390/rs16030591

Adam, E., Mutanga, O., Odindi, J., & Abdel-Rahman, E.M. (2014). Land-use/cover classification in a heterogeneous coastal landscape using RapidEye imagery: Evaluating the performance of random forest and support vector machines classifiers. *International Journal of Remote Sensing*, *35* (10), 3440-3458. https://doi.org/10.1080/01431161.2014.903435

Adugna, T., Xu, W., & Fan, J. (2022). Comparison of random forest and support vector machine classifiers for regional land cover mapping using coarse resolution FY-3C images. *Remote Sensing*, *14* (3), 574. https://doi.org/10.3390/rs14030574

Ahady, A.B., & Kaplan, G. (2022). Classification comparison of Landsat-8 and Sentinel-2 data in Google Earth Engine, study case of the city of Kabul. *International Journal of Engineering and Geosciences*, *7* (1), 24-31. https://doi.org/10.26833/ijeg.860077

Ahmad, A., Sakidin, H., Sari, M.Y.A., Amin, A., Sufahani, S.F., & Rasib, A.W. (2021). Naïve bayes classification of high-resolution aerial imagery. *International Journal of Advanced Computer Science and Applications*, *12* (11). https://doi.org/10.14569/ijacsa.2021.0121120

Aldiansyah, S., & Saputra, R.A. (2022). Comparison of machine learning algorithms for land use and land cover analysis using Google Earth Engine (Case study: Wanggu Watershed). *International Journal of Remote Sensing and Earth Sciences*, *19* (2), 197-210. http://dx.doi.org/10.30536/j.ijreses.2022.v19.a3803

Atasoy, A., & Geçen, R. (2014). Reyhanlı İlçesi topraklarında tuzlanma problemi. *Türk Coğrafya Dergisi, 62,* 21-28.

Bilginer, Ş. (2023). Kuraklığa uyum sürecinde etkili su kullanım yöntemleri ve toprak verimliliğinin iklim-akıllı tarım uygulamaları çerçevesinde incelenmesi: Reyhanlı (Hatay) ilçesi örneği. Yüksek Lisans Tezi, İstanbul Üniversitesi, Sosyal Bilimler Enstitüsü, 104 s.

Bouslihim, Y., Kharrou, M.H., Miftah, A., Attou, T., Bouchaou, L., & Chehbouni, A.G. (2022). Comparing pan-sharpened Landsat-9 and Sentinel-2 for land-use classification using machine learning classifiers. *Journal of Geovisualization and Spatial Analysis*, *6* (35). https://doi.org/10.1007/s41651-022-00130-0

Breiman, L. (2001). Random forests. *Machine Learning*, *45*, 5-32.

Camargo, F.F., Sano, E.E., Almeida, C.M., Mura, J.C., & Almeida, T.D. (2019). A comparative assessment of machine-learning techniques for land use and land cover classification of the Brazilian tropical savanna using ALOS-2/PALSAR-2 polarimetric images. *Remote Sensing*, *11* (13), 1600. https://doi.org/10.3390/rs11131600

Castillo, G.V., de Freitas, L.J., Cordeiro, V.A., Orellana, J.B., Reategui-Betancourt, J., Nagy, L., & Matricardi, E.A. (2022). Assessment of selective logging impacts using UAV, Landsat, and Sentinel data in the Brazilian Amazon rainforest. *Journal of Applied Remote Sensing*, *16* (1), 014526. https://doi.org/10.1117/1.jrs.16.014526

Cerrada, M., Zurita, G., Cabrera, D., Sánchez, R., Artés, M., & Li, C. (2016). Fault diagnosis in spur gears based on genetic algorithm and random forest. *Mechanical Systems and Signal Processing*, 70-71, 87-103. https://doi.org/10.1016/j.ymssp.2015.08.030

Cristóbal, J., Jiménez-Muñoz, J.C., Prakash, A., Mattar, C., Skokovic, D., & Sobrino, J.A. (2018). An improved single-channel method to retrieve land surface temperature from the Landsat-8 thermal band. *Remote Sensing*, *10* (3), 431. https://doi.org/10.3390/rs10030431

Dang, V.H., Hoang, N.D., Nguyen, L.M.D., Bui, D.T., & Samui, P. (2020). A novel GIS-based random forest machine algorithm for the spatial prediction of shallow landslide susceptibility. *Forests*, *11* (1), 118. https://doi.org/10.3390/f11010118

Darem, A.A., Alhashmi, A.A., Almadani, A.M., Alanazi, A.K., & Sutantra, G.A. (2023). Development of a map for land use and land cover classification of the Northern Border Region using remote sensing and GIS. *The Egyptian Journal of Remote Sensing and Space Science*, *26*, 341-350. https://doi.org/10.1016/j.ejrs.2023.04.005

Daribayev, B., Mukhanbet, A.A., Nurakhov, Y., & Imankulov, T. (2021). Implementation of the solution to the oil displacement problem using machine learning classifiers and neural networks. *Eastern-European Journal of Enterprise Technologies*, *5* (4 (113)), 55-63. https://doi.org/10.15587/1729-4061.2021.241858

Deilmai, B.R., Ahmad, B.B., & Zabihi, H. (2014). Comparison of two classification methods (MLC and SVM) to extract land use and land cover in Johor Malaysia. *IOP Conference Series: Earth and Environmental Science*, *20* (1), 012052. https://doi.org/10.1088/1755-1315/20/1/012052

Dhakal, S., Kandel, S., Puri, L., & Shrestha, S. (2022). Assessment on land use land cover mapping: Sentinel-2 versus Landsat-9. *Forestry: Journal of Institute of Forestry, Nepal, 19* (01), 56-63. https://doi.org/10.3126/forestry.v19i01.55704

Fröhlich, B., Bach, E., Walde, I., Hese, S., Schmullius, C., & Denzler, J. (2013). Land cover classification of satellite images using contextual information. *ISPRS Annals of the Photogrammetry, Remote Sensing and Spatial Information Sciences*, *II-3/W1*, 1-6. https://doi.org/10.5194/isprsannals-ii-3-w1-1-2013

Gašparović, M., Zorić, Š., & Singh, S.K. (2021). Urbanisation impact on creation of heat islands in large cities. *The International Archives of the Photogrammetry, Remote Sensing and Spatial Information Sciences*, *XLIII-B3-2021*, 313-318. https://doi.org/10.5194/isprs-archives-xliii-b3-2021-313-2021

Geçen, R. (2019). Uydu görüntüsü kullanılarak tarımsal alanlarda parsel-tabanlı ürün sınıflandırması: Amik Ovası örneği. E Akköprü ve MF Döker (Eds.), *Coğrafya araştırmalarında coğrafi bilgi sistemleri uygulamaları* (1.Baskı, s. 241-266). Pegem.

Ghosh, A., & Joshi, P.K. (2014). A comparison of selected classification algorithms for mapping bamboo patches in lower Gangetic plains using very high resolution WorldView 2 imagery. *International Journal of Applied Earth Observation and Geoinformation*, *26*, 298-311. https://doi.org/10.1016/j.jag.2013.08.011

Gunlu, A. (2021). Comparison of different classification approaches for land cover classification using multispectral and fusion satellite data: A case study in Ören Forest Planning Unit. *Journal of Bartin Faculty of Forestry*, *23* (1), 306-322. https://doi.org/10.24011/barofd.882471

Helber, P., Bischke, B., Dengel, A., & Borth, D. (2019). Eurosat: a novel dataset and deep learning benchmark for land use and land cover classification. *IEEE Journal of Selected Topics in Applied Earth Observations and Remote Sensing*, *12* (7), 2217-2226. https://doi.org/10.1109/jstars.2019.2918242

Htitiou, A., Boudhar, A., Lebrini, Y., Hadria, R., Lionboui, H., Elmansouri, L., Tychon, B., & Benabdelouahab, T. (2019). The performance of random forest classification based on phenological metrics derived from Sentinel-2 and Landsat 8 to map crop cover in an irrigated semiarid region. *Remote Sensing Earth Systems Science*, *2* (4), 208-224. https://doi.org/10.1007/s41976-019-00023-9

Irvem, A., & Ozbuldu, M. (2023). Downscaling of the land surface temperature data obtained at four different dates in a year using the GWR model: a case study in Antakya, Turkey. *Journal of the Indian Society of Remote Sensing*, *51*, 1241-1252. https://doi.org/10.1007/s12524-023-01700-5

Islami, F.A., Tarigan, S., Wahjunie, E.D., & Dasanto, B.D. (2022). Accuracy assessment of land use change analysis using google earth in sadar watershed mojokerto regency. *IOP Conference Series: Earth and Environmental Science*, *950* (1), 012091. https://doi.org/10.1088/1755-1315/950/1/012091

Jamali, A. (2019). Evaluation and comparison of eight machine learning models in land use/land cover mapping using Landsat 8 OLI: a case study of the northern region of Iran. *SN Applied Sciences*, *1*, 1448. https://doi.org/10.1007/s42452-019-1527-8

Jombo, S., & Adelabu, S. (2023). Evaluating Landsat-8, Landsat-9, and Sentinel-2 imageries in land use and land cover (LULC) classification in a heterogeneous urban area. *GeoJournal*, *88* (1), 377-399. https://doi.org/10.1007/s10708-023-10982-8

Khaliq, A., Comba, L., Biglia, A., Aimonino, D.R., Chiaberge, M., & Gay, P. (2019). Comparison of satellite and uav-based multispectral imagery for vineyard variability assessment. *Remote Sensing*, *11* (4), 436. https://doi.org/10.3390/rs11040436

Leeuwen, B.V., Tobak, Z., & Kovács, F. (2020). Comparison of different machine learning techniques for land use/land cover classification of medium resolution optical satellite imagery focusing on temporary inundated areas. *Journal of Environmental Geography*, *13* (1-2), 43-52. https://doi.org/10.2478/jengeo-2020-0005

Li, S., & Xu, X. (2021). Study on remote sensing monitoring model of agricultural drought based on random forest deviation correction. *INMATEH Agricultural Engineering*, 413-422. https://doi.org/10.35633/inmateh-64-41

Ma, L., & Fan, S. (2017). Cure-smote algorithm and hybrid algorithm for feature selection and parameter optimization based on random forests. *BMC Bioinformatics*, *18* (1). https://doi.org/10.1186/s12859-017-1578-z

Manessa, M.D.M., Ummam, M.A.F., Efriana, A.F., Semedi, J.M., & Ayu, F. (2024). Assessing Derawan Island's Coral Reefs over two decades: A machine learning classification perspective. *Sensors*, *24* (2), 466. https://doi.org/10.3390/s24020466

McCorkel, J., Montanaro, M., Efremova, B., Pearlman, A., Wenny, B.N., Lunsford, A., & Reuter, D.C. (2018). Landsat-9 thermal infrared sensor 2 characterization plan overview. *IGARSS 2018 - 2018 IEEE International Geoscience and Remote Sensing Symposium,* Spain, 8845-8848.

Mishra, P.K., Rai, A., & Rai, S.C. (2020). Land use and land cover change detection using geospatial techniques in the Sikkim Himalaya, India. *The Egyptian Journal of Remote Sensing and Space Science*, *23* (2), 133-143. https://doi.org/10.1016/j.ejrs.2019.02.001

Mondal, A., Kundu, S., Chandniha, S.K., Shukla, R., & Mishra, P.K. (2012). Comparison of support vector machine and maximum likelihood classification technique using satellite imagery. *International Journal of Remote Sensing and GIS*, *1* (2), 116-123.

Morgan, G.R., Wang, C., Li, Z., Schill, S.R., & Morgan, D.R. (2022). Deep learning of high-resolution aerial imagery for coastal marsh change detection: a comparative study. *ISPRS International Journal of Geo-Information*, *11* (2), 100. https://doi.org/10.3390/ijgi11020100

Nyamekye, C., Ghansah, B., Agyapong, E., Obuobie, E., Awuah, A., & Kwofie, S. (2021). Examining the performances of true color RGB bands from Landsat-8, Sentinel-2 and UAV as stand-alone data for mapping artisanal and small-scale mining (ASM). *Remote Sensing Applications: Society and Environment*, *24*, 100655. https://doi.org/10.1016/j.rsase.2021.100655

Palanisamy, P.A., Jain, K., & Bonafoni, S. (2023). Machine learning classifier evaluation for different ınput combinations: a case study with Landsat 9 and Sentinel-2 data. *Remote Sensing*, *15* (15), 3241. https://doi.org/10.3390/rs15133241

Paul, S., & Kumar, D.N. (2019). Comparison of Landsat-8 and Sentinel-2 data for classification of Rabi crops over Karnataka, India. *The International Archives of the Photogrammetry, Remote Sensing and Spatial Information Sciences*, *XLII-3/W6*, 579-584. https://doi.org/10.5194/isprs-archives-xlii-3-w6-579-2019

Peng, X., Liu, H., Chen, Y., Qiao, C., Wang, J., Li, H., & Zhao, A. (2021). A method to identify dacrydium pierrei hickel using unmanned aerial vehicle multi-source remote sensing data in a chinese tropical rainforest. *Journal of the Indian Society of Remote Sensing*, *50* (1), 25-35. https://doi.org/10.1007/s12524-021-01453-z

Rakwatin, P., Longépé, N., Isoguchi, O., Shimada, M., & Uryu, Y. (2010). Mapping tropical forest using alos palsar 50m resolution data with multiscale glcm analysis. *2010 IEEE International Geoscience and Remote Sensing Symposium*, USA, 1234-1237. https://doi.org/10.1109/igarss.2010.5651347

Razafinimaro, A., Hajalalaina, A.R., Rakotonirainy, H.L., & Zafimarina, R. (2022). Land cover classification based optical satellite images using machine learning algorithms. *International Journal of Advances in Intelligent Informatics*, *8* (3), 362-380. https://doi.org/10.26555/ijain.v8i3.803

Rwanga, S.S., & Ndambuki, J.M. (2017). Accuracy assessment of land use/land cover classification using remote sensing and GIS. *International Journal of Geosciences*, *8* (4), 611-622. https://doi.org/10.4236/ijg.2017.84033

Saboori, M., Homayouni, S., Shah-Hosseini, R., & Zhang, Y. (2022). Optimum feature and classifier selection for accurate urban land use/cover mapping from very high resolution satellite imagery. *Remote. Sensing*, *14* (9), 2097. https://doi.org/10.3390/rs14092097

Shi, Y., Qi, Z., Li, X., Niu, N., & Zhang, H. (2019). Urban land use and land cover classification using multisource remote sensing images and social media data. *Remote Sensing*, *11* (22), 2719. https://doi.org/10.3390/rs11222719

Simons, G., Bastiaanssen, W., Ngô, L.A., Hain, C., Anderson, M.C., & Senay, G.B. (2016). Integrating global satellite-derived data products as a pre-analysis for hydrological modelling studies: a case study for the red river basin. *Remote Sensing*, *8* (4), 279. https://doi.org/10.3390/rs8040279

Sisodia, P.S., Tiwari, V., & Kumar, A. (2014). Analysis of supervised maximum likelihood classification for remote sensing image. *International Conference on Recent Advances and Innovations in Engineering (ICRAIE-2014)*, India, 1-4. https://doi.org/10.1109/icraie.2014.6909319

Talukdar, S., Singha, P., Mahato, S., Shahfahad, Pal, S., Liou, Y., & Rahman, A. (2020). Land-use land-cover classification by machine learning classifiers for satellite observations - a review. *Remote Sensing*, *12* (7), 1135. https://doi.org/10.3390/rs12071135

Tariq, A., Hong, S.Y., Gagnon, A.S., Li, Q., Mumtaz, F., Hysa, A., & Munir, I. (2021). Assessing burned areas in wildfires and prescribed fires with spectral indices and sar images in the margalla hills of pakistan. *Forests*, *12* (10), 1371. https://doi.org/10.3390/f12101371

Toosi, N.B., Soffianian, A.R., Fakheran, S., Pourmanafi, S., Ginzler, C., & Waser, L.T. (2019). Comparing different classification algorithms for monitoring mangrove cover changes in southern Iran. *Global Ecology and Conservation*, *19*, e00662. https://doi.org/10.1016/j.gecco.2019.e00662

Topaloglu, R.H., Sertel, E., & Musaoğlu, N. (2016). Assessment of classification accuracies of Sentinel-2 and Landsat-8 data for land cover/use mapping. *ISPRS - International Archives of the Photogrammetry, Remote Sensing and Spatial Information Sciences*, 1055-1059. https://doi.org/10.5194/isprsarchives-xli-b8-1055-2016

Tricht, K.V., Gobin, A., Gilliams, S., & Piccard, I. (2018). Synergistic use of Radar Sentinel-1 and Optical Sentinel-2 imagery for crop mapping: a case study for Belgium. *Remote Sensing*, *10*, 1642. https://doi.org/10.3390/rs10101642

Turner, L., Wagner, T.J., Auclair, P., & Langhals, B.T. (2022). Machine learning land cover and land use classification of 4-band satellite imagery. *Faculty Publications, 1407,* 1-17.

Vapnik, V. (2013). *The nature of statistical learning theory (2nd ed.).* Springer. https://doi.org/10.1007/978-1-4757-3264-1

Wang, Y., Ma, J., Xiao, X., Wang, X., Dai, S., & Zhao, B. (2019). Long-term dynamic of Poyang Lake surface water: a mapping work based on the Google Earth Engine cloud platform. *Remote Sensing*, *11* (3), 313. https://doi.org/10.3390/rs11030313

Wei, J., Shang, J., Han, L., Li, X., & Li, X. (2023). Parameter optimization strategy of random forest algorithm for land use classification. *Fourth International Conference on Geoscience and Remote Sensing Mapping (GRSM 2022)*, China, 1255123. https://doi.org/10.1117/12.2668073

Zhang, C., & Li, X. (2022). Land use and land cover mapping in the era of big data. *Land*, *11* (10), 1692. https://doi.org/10.3390/land11101692

Zhang, P., Ke, Y., Zhang, Z., Wang, M., Li, P., & Zhang, S. (2018). Urban land use and land cover classification using novel deep learning models based on high spatial resolution satellite imagery. *Sensors*, *18* (11), 3717. https://doi.org/10.3390/s18113717

Zhao, Y., Gong, P., Yu, L., Hu, L., Li, X., Li, C., Zhang, H., Zheng, Y., Wang, J., Zhao, Y., Cheng, Q., Liu, C., Liu, S., & Wang, X. (2014). Towards a common validation sample set for global land-cover mapping. *International Journal of Remote Sensing*, *35* (13), 4795-4814. https://doi.org/10.1080/01431161.2014.930202

Zhu, Z., Woodcock, C.E., Rogan, J., & Kellndorfer, J. (2012). Assessment of spectral, polarimetric, temporal, and spatial dimensions for urban and peri-urban land cover classification using Landsat and SAR data. *Remote Sensing of Environment*, *117*, 72-82. https://doi.org/10.1016/j.rse.2011.07.020